

The Abiotic Nitrite Oxidation by Ligand-Bound Manganese (III): The Chemical Mechanism

Cite this article as: George W. Luther III, Jennifer S. Karolewski, Kevin M. Sutherland, Colleen M. Hansel and Scott D. Wankel, The Abiotic Nitrite Oxidation by Ligand-Bound Manganese (III): The Chemical Mechanism, Aquatic Geochemistry <https://doi.org/10.1007/s10498-021-09396-0>

This Author Accepted Manuscript is a PDF file of an unedited peer-reviewed manuscript that has been accepted for publication but has not been copyedited or corrected. The official version of record that is published in the journal is kept up to date and so may therefore differ from this version.

Terms of use and reuse: academic research for non-commercial purposes, see here for full terms. <https://www.springer.com/aam-terms-v1>

Author accepted manuscript

The abiotic nitrite oxidation by ligand-bound manganese (III): the chemical mechanism

George W. Luther, III^{a,*}, Jennifer S. Karolewski^{b,c}, Kevin M. Sutherland^d, Colleen M. Hansel^b
and Scott D. Wankel^b

^aSchool of Marine Science & Policy, University of Delaware, Lewes, DE 19958, United States

^bDepartment of Marine Chemistry and Geochemistry, Woods Hole Oceanographic Institution,
Woods Hole, MA 02540, United States

^cDepartment of Earth, Atmospheric and Planetary Sciences, Massachusetts Institute of
Technology, Cambridge, MA 02139, United States

^dDepartment of Earth and Planetary Sciences, Harvard University, Cambridge, MA 02138,
United States

*Corresponding author.

E-mail address: luther@udel.edu (G. W. Luther)

Abstract

Given their environmental abundances, it has been long hypothesized that geochemical interactions between reactive forms of manganese and nitrogen may play important roles in the cycling of these elements. Indeed recent studies have begun shedding light on the possible role of soluble, ligand bound Mn(III) in promoting abiotic transformations under environmentally relevant conditions. Here, using the kinetic data of Karolewski et al. (2021), we provide the chemical mechanism for the abiotic oxidation of nitrite (NO_2^-) by Mn(III)-pyrophosphate, $\text{Mn}^{\text{III}}\text{PP}$, to form nitrate (NO_3^-). Nitrous acid (HNO_2), not NO_2^- , is the reductant in the reaction, based on thermodynamic and kinetic considerations. As soluble Mn(III) complexes react in a one-electron transfer reaction, two one-electron transfer steps must occur. In step one, HNO_2 is first oxidized to nitrogen dioxide, $\bullet\text{NO}_2$, a free radical via a hydrogen atom transfer (HAT) reaction. We show that this inner sphere reaction process is the rate limiting step in the reaction sequence. In step two, $\bullet\text{NO}_2$ reacts with a second $\text{Mn}^{\text{III}}\text{PP}$ complex to form the nitronium ion (NO_2^+), which is isoelectronic with CO_2 . Unlike the poor electron accepting capability of CO_2 , NO_2^+ is an excellent electron acceptor for both OH^- and H_2O , so NO_2^+ reacts quickly with water to form the end-product NO_3^- (step 3 in the reaction sequence). Thus, water provides the O atom in this nitrification reaction in accordance with the O-isotope data. This work provides mechanistic perspective on a potentially important interaction between Mn and nitrogen species, thereby offering a framework in which to interpret kinetic and isotopic data and to further investigate the relevance of this reaction under environmental conditions.

1. INTRODUCTION

Links among various elemental cycles are a hallmark of biogeochemical complexity across Earth's biosphere. Further, biogeochemical interactions between elemental cycles are driven by complex networks of both biological and chemical reactions often operating within close proximity, making it difficult to disentangle their relative roles. For example, while very few reports exist of microorganisms directly coupling energy-gaining redox reactions between manganese (Mn) and nitrogen (N), repeated evidence has emerged from redox gradients in natural sediments for the chemical coupling of Mn reduction to oxidation of N species (e.g., Luther et al 1997; Lin and Taillefert 2014; Anschutz et al. 2000). The work on the chemical mechanism for abiotic Mn/N reactions is limited to the abiotic nitrification reaction of nitrite species with MnO₂ (Luther and Popp 2002) and to the oxidation of NH₂OH to N₂O by MnO₂ (Cavazos et al. 2018). This is in contrast to the work on chemical mechanisms of solid-phase oxidized Mn (e.g., MnO₂) with other reductants; e.g. H₂S (Herzsage and Afonso 2003; Yao and Millero 1993, 1995; Luther et al. 2018), organic compounds (Matocha et al 2001; Stone and Morgan 1984 a b), and As(III) (Owings et al. 2019). Interestingly, all these studies did not include isotope studies although they discussed electron transfer, intermediates, and molecular mechanisms.

Recently Karolewski et al. (2021) performed a study on the reaction of Mn(III)-pyrophosphate [Mn^{III}PP] with nitrite leading to the formation of nitrate (eq. 1); an abiotic nitrification reaction.



The experimental details were well documented, and the results show a rate law as in eq. 2.

$$\frac{d}{dt} [NO_3^-] = k[Mn^{III}PP]^2 [HNO_2] \quad (2)$$

The reported isotope data also clearly demonstrated that the additional O atom in the product nitrate originated from water, the solvent, as also indicated in eq. 1. Their nitrogen isotope data exhibited an inverse N isotope effect, which while unusual is consistent with that occurring during microbial nitrite oxidation observed directly in culture studies as well as inferred from field measurements in several oxygen deficient zones (ODZ) and sediment porewaters (Buchwald and Casciotti 2013; Casciotti, 2009, 2016). Mn(III)-ligand complexes are found in many environmentally relevant redox transition zones, such as ODZs, constituting a substantial fraction of the dissolved Mn pool (Trouwborst et al. 2006; Oldham et al. 2015, 2017a; Delwig et al. 2012). As the kinetics of the various abiotic and biotic nitrite oxidation reactions are similar, oxidized Mn could be at least partly responsible for the conversion of nitrite to nitrate within environmental systems.

The focus of Karolewski et al. (2021) was primarily on regulation of reaction rates and isotope dynamics, and did not address possible chemical reaction mechanisms, including electron transfer processes, the formation of any intermediates ($\bullet NO_2$, NO_2^+) and how the O atom comes from water to form NO_3^- . Their rate law suggests that the oxidation of nitrite must occur via two 1-electron transfers as Mn(III) can only accept one electron; nevertheless, they did not describe any electron transfers or intermediates. Here, using the recently reported kinetic and isotope data together with thermodynamic data from other works, we provide a more developed description

of the redox processes involved, including the specific chemical species that react at different pH values and the steps of reaction progress that include intermediates. Lastly, we perform an analysis of the molecular structure and molecular orbital properties of the reactants and intermediates to describe chemical mechanisms for each step of the reaction progress.

2. RESULTS

The thermodynamics of the reactions over a range of pH values leads to mechanistic details of the reaction and are described first. We show that there are three steps to the overall reaction, which involves the transformation of HNO_2 to $\bullet\text{NO}_2$ to NO_2^+ to the endproduct, NO_3^- .

2.1. Two one-electron transfer steps

Because eq. 1 starts with a complex of Mn(III), HNO_2 or NO_2^- must act as a 1-electron transfer reductant. Here, we summarize the relevant reaction progress of two 1-electron transfer steps as going from NO_2^- to $\bullet\text{NO}_2$ to NO_3^- using thermodynamics and kinetics. The electron transfer must be inner sphere for Mn as there is a mismatch of symmetry for the highest occupied molecular orbital (HOMO) of NO_2^- (π^* orbital) and the lowest unoccupied molecular orbital (LUMO) of Mn(III) (σ orbital) (Luther et al. 2005; Luther 2016). The first step in the reaction is likely a hydrogen atom transfer reaction (HAT). Recently, Luther et al. (2018) described HAT reactions for the reduction of MnOOH , MnO_2 and HNO_2 by leucoberbelein blue (LBB). The reaction is pH independent for MnO_2 (a two-electron oxidant) and pH dependent for the one-electron oxidants MnOOH and HNO_2 (Jones et al. 2019; Luther et al. 2018). HAT reactions for LBB are a function of the C-H homolytic bond dissociation energy (BDE) for triphenylmethane compounds that ranges from 293 to 335 kJ mol^{-1} (Zhang and Bordwell 1992). If the

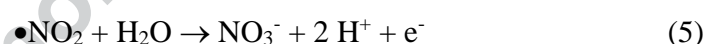
thermodynamics of the oxidized Mn reduction half-reactions are more negative than the BDE value, the reaction is favorable. The O-H homolytic bond dissociation energy for HNO₂ is 329 kJ mol⁻¹ (Bach et al. 1996) so HNO₂ can react with oxidized Mn in a similar manner to LBB.

2.2. Thermodynamics of the nitrogen species HNO₂, •NO₂ and NO₃⁻ over a range of pH

Oxidation of nitrite to nitrate by soluble Mn(III) compounds occurs via two sequential one-electron transfers according to the stoichiometry in eq. 1 and can be represented by the following two equations that represent the first (eqs. 3, 4) and second electron transfer steps (eq. 5). As will be shown below and as was shown for the reaction of MnO₂ with nitrite (Luther and Popp, 2002), oxidation of HNO₂ is thermodynamically favored over NO₂⁻. The free radical nitrogen dioxide, •NO₂, is the expected metastable intermediate. Equations 3 and 5 demonstrate the pH dependence of the overall reaction as previously reported (Karolewski et al. 2021).



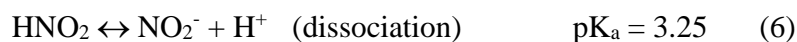
A HAT reaction, which is analogous to eq. 3, is represented by eq. 4 (Luther et al. 2018).



There is also a mismatch of orbital symmetry for •NO₂ (the intermediate formed after the loss of the first electron from nitrite) and Mn(III), also indicating that this reaction is an inner sphere electron transfer.

2.3. Thermodynamics of HNO₂ (NO₂⁻), •NO₂, NO₃⁻ redox half-reactions and acid dissociation

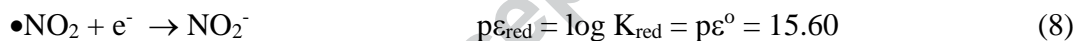
From Luther (2010, 2016) and Luther and Popp (2002), we have the following acid dissociation (eq. 6) reaction, and redox half-reactions with their thermodynamic functions over pH (eqs. 7-9).



The redox half-reactions and calculations are at *standard state conditions* and potentials are given versus the normal hydrogen electrode (NHE). The first electron transfer will be shown to be the rate limiting step and is a function of pH. We write the redox half-reactions as reduction reactions noting that the reverse (oxidation) half-reactions ('a') are operative for the processes discussed here. The reverse half-reaction, $\text{p}\epsilon_{\text{oxid}}$, is eq. 7a and occurs during $\text{Mn}^{\text{III}}\text{PP}$ reduction (see eqs. 3-5).

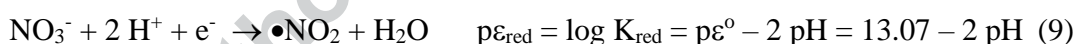


$$\text{p}\epsilon_{\text{oxid}} = \log K_{\text{oxid}} = -\text{p}\epsilon^\circ + \text{pH} = -16.51 + \text{pH} \quad (7a)$$



$$\text{p}\epsilon_{\text{oxid}} = \log K_{\text{oxid}} = -15.60 \quad (8a)$$

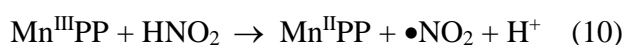
The half-reaction for the reduction of NO_3^- to $\bullet\text{NO}_2$ (the second electron transfer step) is eq. 9.



$$\text{p}\epsilon_{\text{oxid}} = \log K_{\text{oxid}} = 2\text{pH} - 13.07 \quad (9a)$$

2.4. Thermodynamics of the Mn^{III} pyrophosphate, $\text{Mn}^{\text{III}}\text{PP}$, reduction half-reaction

The general equation for the first electron transfer of HNO_2 , which will be shown to be rate limiting, is given in eq. 10. Eq. 10a using NO_2^- as reductant will be shown to be unfavorable.



The second electron transfer is given by eq. 11 (11a).



To calculate thermodynamic favorability of these reactions requires data on the reduction of $\text{Mn}^{\text{III}}\text{PP}$ to $\text{Mn}^{\text{II}}\text{PP}$ (eq. 12).



Watters and Kolthoff (1948, see their Table 3) measured Mn(III) reduction potentials versus the saturated calomel electrode (SCE) for $\text{Mn}^{\text{III}}\text{PP}$ species (see column 3 of our Table 1) over the pH range from 0.05 to 8.72. In their work, total concentrations of Mn(III) and Mn(II) were 5 mM, and the total concentration of pyrophosphate was 0.4 M at each pH. Their SCE potentials were converted to potentials versus NHE (column 4 of Table 1) from which the equilibrium constant, K_{red} , and $p\varepsilon_{\text{red}}$ (see column 5 of Table 1) of the half-reaction could be calculated.

Watters and Kolthoff (1948) also provided information on the protonation of the pyrophosphate ligand over pH. At pH < 3, the complex is $[\text{Mn}^{\text{III}}(\text{H}_2\text{P}_2\text{O}_7)_3]^{3-}$ and above pH 6, it is $[\text{Mn}^{\text{III}}(\text{HP}_2\text{O}_7)_3]^{9-}$ as several H^+ are lost on increasing pH. Thus, both $\text{Mn}^{\text{III}}\text{PP}$ and nitrite speciation vary with pH, and both species will lose H^+ as pH increases (see Figure 1).

The thermodynamics for the reactions represented by equations 10 and 11 can now be calculated to predict the favorability of the reaction over a range of pH values. The thermodynamics of equation 10 (column 6 in Table 1) is calculated from the sum of eq. 7a (column 2 in Table 1) and eq. 12 (column 5 in Table 1), which is eq. 13.

$$\Delta \log K_{\text{reaction}} = p\varepsilon_{\text{red}} (\text{Mn}^{\text{III}}\text{PP}) + p\varepsilon_{\text{oxid}} (\text{HNO}_2) \quad (13)$$

$$\Delta \log K_{\text{reaction}} = p\varepsilon_{\text{red}} (\text{Mn}^{\text{III}}\text{PP}) + p\varepsilon_{\text{oxid}} (\text{NO}_2^-) \quad (13a)$$

Column 6 in Table 1 shows that the reaction (from eqs. 10, 13) is favorable ($\Delta \log K_{\text{reaction}} > 0$) at pH values $< \sim 4.3$ (see also Figure 1).

The first electron transfer using NO_2^- (column 7 in Table 1) rather than HNO_2 shows that NO_2^- is not as favorable as an oxidant for $\text{Mn}^{\text{III}}\text{PP}$ (last column of Table 1; eq. 10a) as HNO_2 . Here, $\Delta \log K_{\text{reaction}}$ data (addition of columns 5 and 7; eq. 13a) indicate that the reaction of $\text{Mn}^{\text{III}}\text{PP}$ with NO_2^- to form $\bullet\text{NO}_2$ is favorable only at low pH (< 2.3), where NO_2^- is not the dominant chemical species according to eq. 6 (see also section 3.2). Thus, NO_2^- is not the reductant for $\text{Mn}^{\text{III}}\text{PP}$. These data parallel the thermodynamic data found for the 2-electron reduction of MnO_2 by HNO_2 to form NO_3^- (Luther and Popp 2002) where the nitrate formation reaction rate also decreased with increasing pH.

Table 1. Prediction of thermodynamic favorability for the reaction $\text{Mn}^{\text{III}}\text{PP} + \text{HNO}_2 \rightarrow \text{Mn}^{\text{II}}\text{PP} + \bullet\text{NO}_2 + \text{H}^+$ (Column 6, eq. 10) and $\text{Mn}^{\text{III}}\text{PP} + \text{NO}_2^- \rightarrow \text{Mn}^{\text{II}}\text{PP} + \bullet\text{NO}_2$ (Column 8, eq. 10a).

Values of $\Delta\log K_{\text{reaction}}$ (columns 6 and 8) that are positive and in bold font indicate a favorable reaction whereas values in *italic font* indicate an unfavorable reaction.

1) pH	2) $p\epsilon_{\text{oxid}} = \log K_{\text{oxid}}$ for 1 st electron transfer $\text{HNO}_2 \rightarrow \text{NO}_2$ (eq. 7a)	3) E (volt) vs SCE $\text{Mn}^{\text{III}}\text{PP} \rightarrow \text{Mn}^{\text{II}}\text{PP}$	4) E (volt) vs NHE $\text{Mn}^{\text{III}}\text{PP} \rightarrow \text{Mn}^{\text{II}}\text{PP}$	5) $p\epsilon_{\text{red}} = \log K_{\text{red}}$ $\text{Mn}^{\text{III}}\text{PP} \rightarrow \text{Mn}^{\text{II}}\text{PP}$	6) $\Delta\log K_{\text{reaction}} = p\epsilon_{\text{red}} + p\epsilon_{\text{oxid}}$ for $\text{Mn}^{\text{III}}\text{PP}$ reduction/ HNO_2 oxidation	7) $p\epsilon_{\text{oxid}} = \log K_{\text{oxid}}$ for 1 st electron transfer $\text{NO}_2^- \rightarrow \bullet\text{NO}_2$	8) $\Delta\log K_{\text{reaction}} = p\epsilon_{\text{red}} + p\epsilon_{\text{oxid}}$ for $\text{Mn}^{\text{III}}\text{PP}$ reduction/ NO_2^- oxidation
0.05	-16.46	0.9462	1.187	20.13	3.67	15.60	4.53
0.19	-16.32	0.9345	1.176	19.93	3.61	15.60	4.33
0.52	-15.99	0.9035	1.145	19.40	3.41	15.60	3.80
0.8	-15.71	0.8796	1.121	19.00	3.29	15.60	3.40
1.12	-15.39	0.8610	1.102	18.68	3.29	15.60	3.08
1.52	-14.99	0.8260	1.067	18.09	3.10	15.60	2.49
1.76	-14.75	0.8124	1.054	17.86	3.11	15.60	2.26
1.97	-14.54	0.7887	1.030	17.46	2.92	15.60	1.86
2.27	-14.24	0.7584	0.9996	16.94	2.70	15.60	1.34
2.99	-13.52	0.6680	0.9092	15.41	1.89	15.60	<i>-0.19</i>
3.59	-12.92	0.5780	0.8192	13.88	0.96	15.60	<i>-1.72</i>
4.02	-12.49	0.5185	0.7597	12.88	0.39	15.60	<i>-2.72</i>
4.54	-11.97	0.4282	0.6694	11.35	<i>-0.62</i>	15.60	<i>-4.25</i>
5.85	-10.66	0.3184	0.5596	9.48	<i>-1.18</i>	15.60	<i>-6.12</i>
7.11	-9.40	0.2623	0.5035	8.53	<i>-0.87</i>	15.60	<i>-7.07</i>
8.72	-7.79	0.1870	0.4282	7.26	<i>-0.53</i>	15.60	<i>-8.34</i>

Similarly, the thermodynamic favorability of equation 11 is calculated from the sum of eq. 9a (column 2 in Table 2) and eq. 12 (column 3 in Table 2), which is eq. 14.

$$\Delta\log K_{\text{reaction}} = p\epsilon_{\text{red}} (\text{Mn}^{\text{III}}\text{PP}) + p\epsilon_{\text{oxid}} (\bullet\text{NO}_2) \quad (14)$$

The fourth column in Table 2 shows that the reaction is favorable ($\Delta\log K_{\text{reaction}} > 0$) at pH values up to 8.72 (see also Figure 1). Thus, the reaction of $\text{Mn}^{\text{III}}\text{PP}$ with $\bullet\text{NO}_2$ to NO_3^- is favorable over all pH conditions considered.

Table 2. Prediction of thermodynamic favorability for the reaction $\text{Mn}^{\text{III}}\text{PP} + \bullet\text{NO}_2 + \text{H}_2\text{O} \rightarrow \text{Mn}^{\text{II}}\text{PP} + \text{NO}_3^- + 2 \text{H}^+$ (Column 4, eq. 11). Values of $\Delta\log K_{\text{reaction}}$ that are positive and in bold font indicate a favorable reaction.

1) pH	2) $p\varepsilon_{\text{oxid}} = \log K_{\text{oxid}}$ for 2 nd electron transfer $\bullet\text{NO}_2 \rightarrow \text{NO}_3^-$	3) $p\varepsilon_{\text{red}} = \log K_{\text{red}}$ $\text{Mn}^{\text{III}}\text{PP} \rightarrow \text{Mn}^{\text{II}}\text{PP}$	4) $\Delta\log K_{\text{reaction}} = p\varepsilon_{\text{red}} + p\varepsilon_{\text{oxid}}$ for $\text{Mn}^{\text{III}}\text{PP}$ reduction/ $\bullet\text{NO}_2$ oxidation
0.05	-13.02	20.13	7.11
0.19	-12.88	19.93	7.05
0.52	-12.55	19.40	6.85
0.8	-12.27	19.00	6.73
1.12	-11.95	18.68	6.73
1.52	-11.55	18.09	6.54
1.76	-11.31	17.86	6.55
1.97	-11.10	17.46	6.36
2.27	-10.80	16.94	6.14
2.99	-10.08	15.41	5.33
3.59	-9.48	13.88	4.40
4.02	-9.05	12.88	3.83
4.54	-8.53	11.35	2.82
5.85	-7.22	9.48	2.26
7.11	-5.96	8.53	2.57
8.72	-4.35	7.26	2.91

3. DISCUSSION

3.1. Concentration dependence of HNO_2 as the reductant

The $\Delta\log K_{\text{reaction}}$ values in columns 6 (eq. 10) and 8 (eq. 10a) of Table 1 and in column 4 (eq. 11) of Table 2 are plotted versus pH in Figure 1. These data again demonstrate that HNO_2 is the reactant and not NO_2^- . The first electron transfer reaction with HNO_2 as the reductant is favorable up to a pH of 4.3, and then becomes slightly inhibited due to thermodynamics. Thus, this is the rate determining step in the reaction of HNO_2 with $\text{Mn}^{\text{III}}\text{PP}$ to form NO_3^- . The second electron transfer reaction with $\bullet\text{NO}_2$ as the reductant has no thermodynamic barrier at these pH

values. Thus, this step is likely fast and not rate inhibiting. It is at this point that O atoms from water are added to form nitrate.

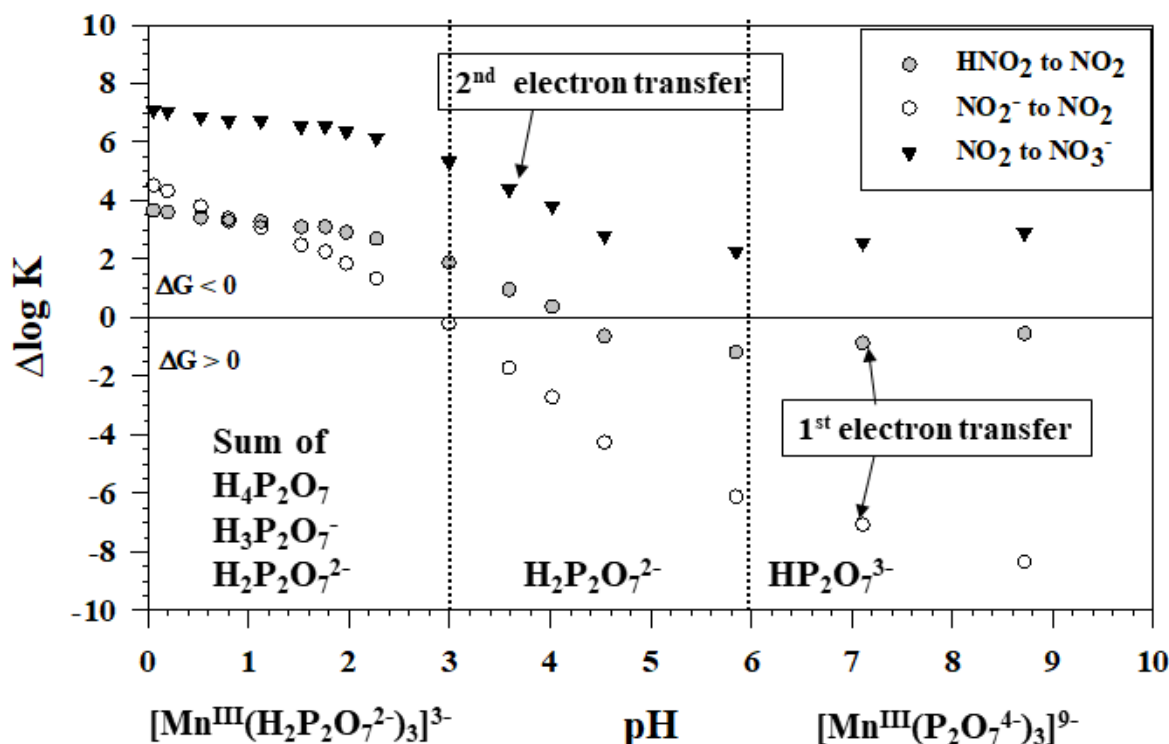


Figure 1. Thermodynamics of Mn^{III}PP reduction over pH by nitrite species and nitrogen dioxide. The vertical lines indicate the predominant pyrophosphate species noted by Watters and Kolthoff (1948). They also indicated the change in Mn^{III}PP speciation with increasing pH as H⁺ dissociates from the pyrophosphate species

The thermodynamic functions 7 and 7a can be expanded as in eqs. 15 and 15a to include the concentrations of HNO₂ and •NO₂. Because •NO₂ is a free radical and its reaction with Mn^{III}PP is favorable over all pH values considered, it likely quickly reacts. The •NO₂ concentration does not buildup so is negligible at any time point; thus, eq. 15b is the relevant half-reaction for calculation of thermodynamic favorability.

$$p\varepsilon_{\text{red}} = \log K_{\text{red}} = p\varepsilon^{\circ} - \text{pH} = 16.51 - \text{pH} + \log [\text{HNO}_2] - \log[\bullet\text{NO}_2] \quad (15)$$

$$p\varepsilon_{\text{oxid}} = \log K_{\text{oxid}} = -p\varepsilon^{\circ} + \text{pH} = -16.51 + \text{pH} - \log [\text{HNO}_2] + \log[\bullet\text{NO}_2] \quad (15a)$$

$$p\varepsilon_{\text{oxid}} = -p\varepsilon^{\circ} + \text{pH} = -16.51 + \text{pH} - \log [\text{HNO}_2] \quad (15b)$$

At pH 7.11 and a total nitrite concentration of 100 μM as done in the work of Karolewski et al. (2021), αHNO_2 (i.e. the fraction of nitrite existing in the protonated form) is 1.41×10^{-4} , so $[\text{HNO}_2]$ equals 1.41×10^{-8} M (or 14.1 nM). From the calculations below (note that the measured $p\varepsilon_{\text{red}}$ includes Mn concentrations), the reaction is thermodynamically favorable at the conditions of the experiments in Karolewski et al. (2021), but slow due to the trace concentration of HNO_2 .

$$p\varepsilon_{\text{oxid}}(\text{HNO}_2) = -16.51 + 7.11 - (-7.85) = -1.56$$

$$p\varepsilon_{\text{red}}(\text{Mn}^{\text{III}}\text{PP}) = 8.53$$

$$\Delta \log K_{\text{reaction}} = p\varepsilon_{\text{oxid}} + p\varepsilon_{\text{red}} = 6.7$$

The vertical lines in Figure 1 indicate the predominant pyrophosphate species noted by Watters and Kolthoff (1948). They also indicated the change in $\text{Mn}^{\text{III}}\text{PP}$ speciation with increasing pH as H^+ dissociates from the pyrophosphate species. They indicated that the solution color changes from intense violet at $\text{pH} < 3$ where $[\text{Mn}^{\text{III}}(\text{H}_2\text{P}_2\text{O}_7^{2-})_3]^{3-}$ dominates speciation to less intense violet above pH 3. The solution color changes to amber starting at pH 4.5 and brown-amber as the pH approaches 7, where $[\text{Mn}^{\text{III}}(\text{P}_2\text{O}_7^{4-})_3]^{9-}$ dominates speciation. These color changes are consistent with stronger metal-ligand bonding and ligand to metal charge transfer transitions (Luther, 2016). Stronger metal-ligand bonding with increased pH also results in less positive or

more negative redox potentials (see data in column 3, Table 1), which make the HNO_2 reaction less favorable as observed. In alkaline solutions of $\text{pH} > 9$, OH^- attacks $[\text{Mn}^{\text{III}}(\text{P}_2\text{O}_7^{4-})_3]^{9-}$ and leads to the disproportionation of the MnPP complex to Mn(II) and MnO_2 (Klewicki and Morgan, 1998; Qian et al, 2019; Watters and Kolthoff 1948). At low pH and in the presence of excess pyrophosphate to Mn as done by Karolewski et al. (2021), the complexes are stable to disproportionation (Klewicki and Morgan, 1998).

3.2. Kinetics data compared with the concentration of HNO_2 over pH

Figure 2A shows the $\text{HNO}_2/\text{NO}_2^-$ species diagram over pH and indicates that there is still a minor amount of HNO_2 at higher pH for reaction with $\text{Mn}^{\text{III}}\text{PP}$. Karolewski et al. (2021) documented a slow reaction at $\text{pH} > 7$. In fact, the nitrite oxidation rate data from Table 2 in Karolewski et al. (2021) follows the speciation of HNO_2 not NO_2^- . Here, both the Figure 2A inset and Figure 2B document that as the fraction of HNO_2 decreases in solution, the nitrite oxidation rate decreases. Our Figure 2A shows similar curves for the fraction of species and reaction rates reported in Luther and Popp (2002) and Luther et al. (2018) for the 2-electron transfer between HNO_2 and MnO_2 ; however, that mechanism was postulated to be a O atom transfer from MnO_2 to HNO_2 .

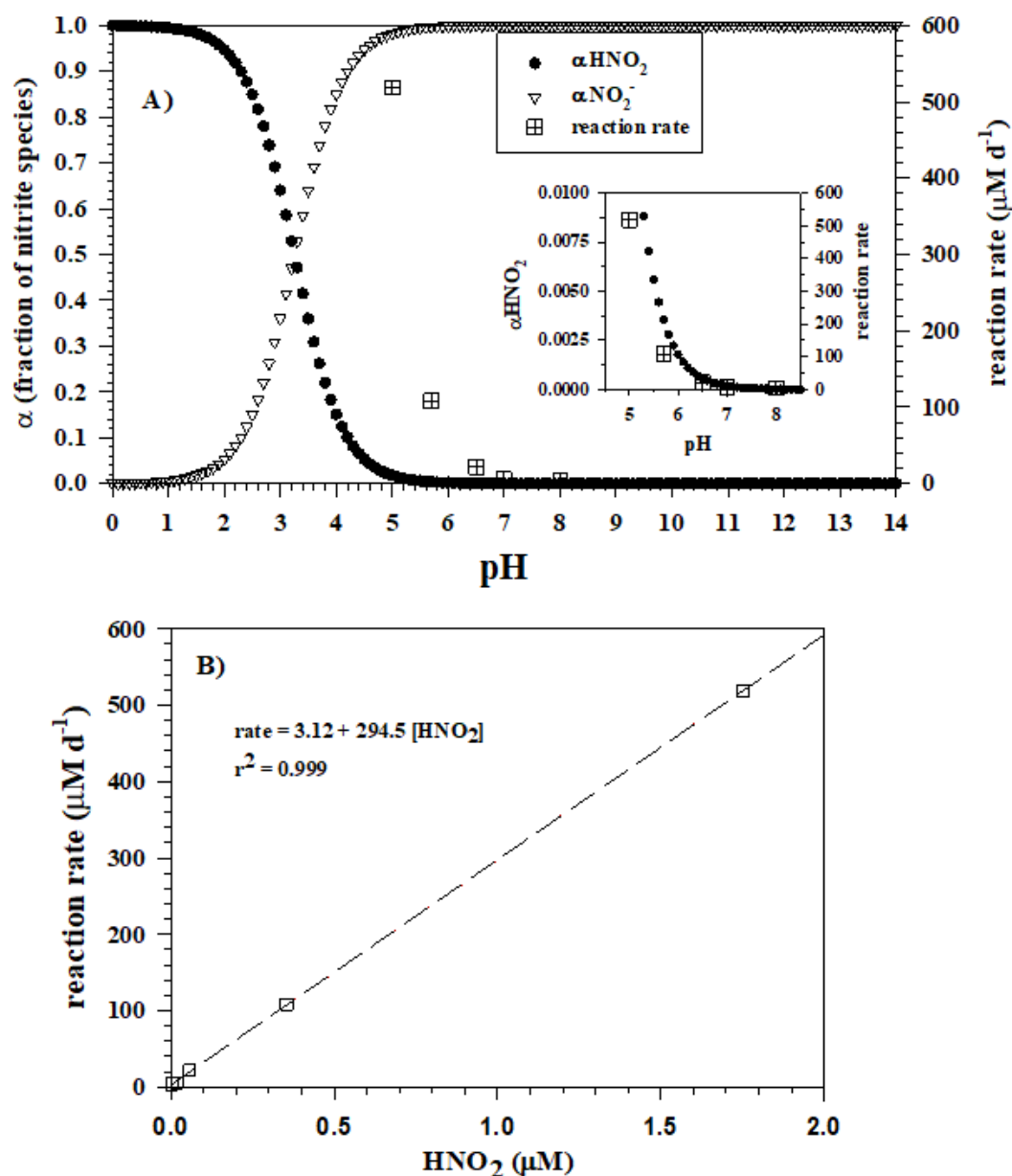


Figure 2. A) Nitrite species diagram versus pH. The inset shows that the nitrite oxidation rate [taken from Table 2 in Karolewski et al. (2021)] increases with the fraction (concentration) of HNO_2 (αHNO_2). B) Nitrite oxidation rate increases linearly with $[\text{HNO}_2]$ (calculated by multiplying αHNO_2 by the concentration of nitrite of 100 μM used in Karolewski et al. 2021).

3.3. Chemical mechanism for the nitrite to nitrate transformation

Here, we use the Lewis Structures for HNO_2 , $\bullet\text{NO}_2$, NO_2^+ and NO_3^- to describe the complete oxidation of HNO_2 to NO_3^- . Equations 3 and 5 above describe the oxidation of HNO_2 to $\bullet\text{NO}_2$ to NO_3^- . However, we also note that there is a short lived intermediate that forms, but which is not represented in these equations. Figure 3 shows two schemes for the complete oxidation and transformation of NO_2^- to NO_3^- . Scheme 1 shows the conversion of HNO_2 to $\bullet\text{NO}_2$ via a one-electron transfer. The one-electron oxidation of $\bullet\text{NO}_2$ leads to formation of the intermediate NO_2^+ , which is isoelectronic with CO_2 . Just as CO_2 can react with H_2O and OH^- to form H_2CO_3 / HCO_3^- , NO_2^+ reacts with H_2O and OH^- to form HNO_3 / NO_3^- as in Scheme 2 of Figure 3 (eqs. 16, 16a). Thus, the O atom comes from water in a Lewis acid-base reaction as found with the O-isotope data from Karolewski et al. (2021). Note that loss of H^+ from H_2O increases on oxidation of HNO_2 .



Overall, the N species reaction pathway is from HNO_2 to $\bullet\text{NO}_2$ to NO_2^+ to NO_3^- .

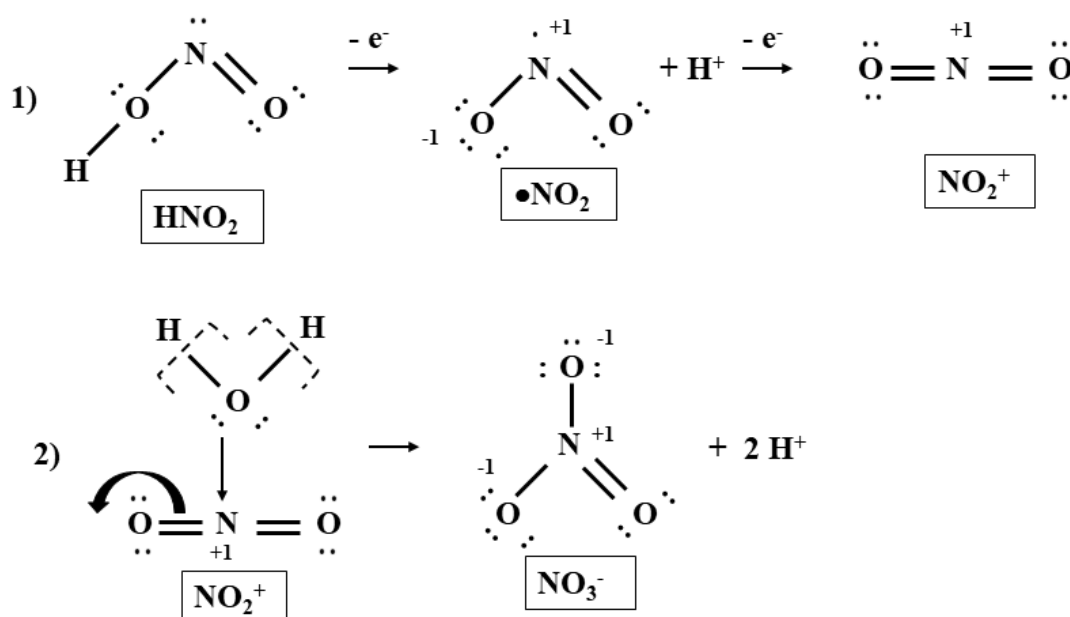


Figure 3. Lewis Structures including formal charges on each atom showing the conversion of NO₂⁻ to •NO₂ to NO₂⁺ in scheme 1. Scheme 2 shows that a bond between the O atom in H₂O forms with the N in NO₂⁺; the dashed brackets indicate the electrons from the H-O bonds in H₂O remain with the O atom when H⁺ dissociates, and the curved arrow indicates one of the pairs of electrons in the O=N double bond moves to the O atom so NO₃⁻ results.

3.4. Energetics and reactivity of NO₂⁺ as a transient intermediate

Unlike the slow kinetics at low pH for the reaction of CO₂ with H₂O to form H₂CO₃, the reaction of NO₂⁺ with H₂O is fast enough to promote nitrate formation at low pH. Figure 4 shows the energies of the HOMO and LUMO orbitals (tabulated in Luther 2016) for the relevant species described in this paper. The LUMO energy for NO₂⁺ is equivalent to the reverse of the ionization potential of •NO₂ (experimental value is 9.75 eV) so the LUMO value is -9.75 eV. Thus, NO₂⁺, which has a positive N atom, is an excellent electron acceptor in contrast to CO₂, which has a LUMO experimental value of +0.5 eV indicating it is a poor electron acceptor (Luther 2004).

Although the H₂O HOMO energy is -12.61 eV, this difference of 2.86 eV between the E_{HOMO} of H₂O and the E_{LUMO} of NO₂⁺ is an acceptable uphill energy of activation, E_a (Luther 2016). This uphill E_a is similar to that found for the reaction of OH⁻ with CO₂ (2.325 eV) to form HCO₃⁻. In contrast, the OH⁻ HOMO of -1.825 eV gives a downhill reaction with NO₂⁺ and an energy difference of -7.925 eV; thus, there is no E_a.

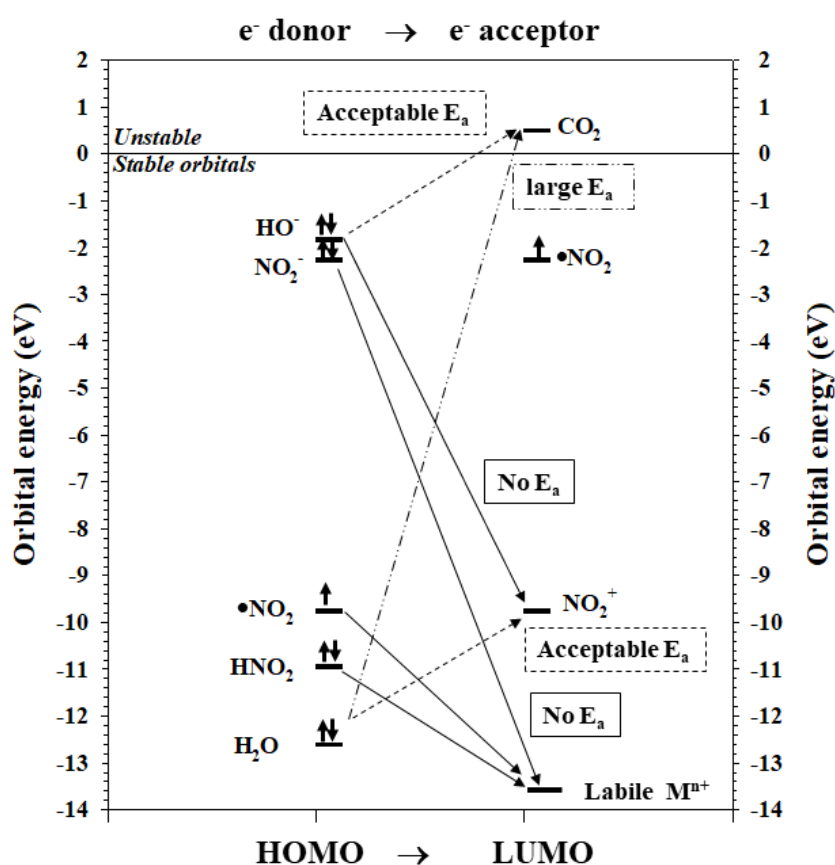


Figure 4. Energies for the HOMO and LUMO orbitals of the various reactants. The HNO₂ data point is from Hoener et al. (2021). Good electron donors have more positive E_{HOMO} values whereas good electron acceptors have more negative E_{LUMO} values.

Also, the species OH^- , H_2O , HNO_2 and NO_2^- have HOMO energies that permit the ease of donation of a pair of electrons to a labile Mn(III) complex or a vacant coordination site to form a Mn-O bond. Thus, an inner sphere complex can form prior to electron transfer, which is required for the orbital symmetry mismatch for the HOMO of HNO_2 and the LUMO of Mn(III) . The LUMO energies for most transition metals that are labile are more negative than -14 to -15 eV so are excellent electron acceptors (Luther 2016). For Mn(III) complexes with a d^4 or $t_{2g}^3 e_g^1$ electron configuration for octahedral complexes, Jahn-Teller distortion occurs which leads to labile complexes and attack of Mn(III) by an electron pair donor (ligand). Here, because of distortion, one O atom from a pyrophosphate ligand can dissociate from Mn(III) for HNO_2 to attack. At alkaline pH, hydroxide ion, which is increased in concentration and is a stronger nucleophile than the N species in Figure 4, outcompetes the N species for the Mn in $\text{Mn}^{\text{III}}\text{PP}$. Thus, disproportionation of $\text{Mn}^{\text{III}}\text{PP}$ occurs yielding Mn(II) and MnO_2 .

4. CONCLUSIONS

Using the kinetic and isotope data from Karolewski et al. (2021) as well as known thermodynamic data for the speciation of the reactants, we show that HNO_2 is the reactant with $\text{Mn}^{\text{III}}\text{PP}$ to form NO_3^- . Using the molecular properties of the intermediate N species ($\bullet\text{NO}_2$ and NO_2^+), we show that the O atom must come from H_2O in agreement with the isotope data. The first intermediate formed is $\bullet\text{NO}_2$, which on losing an electron to reduce $\text{Mn}^{\text{III}}\text{PP}$ forms NO_2^+ , which in turn reacts with H_2O to form NO_3^- .

The investigation of reactions of Mn(III) complexes for environmental applications have been few. Despite the favorable thermodynamic conditions for reactions coupling Mn and N

transformations, direct evidence for the occurrence of these reactions in natural systems remains limited. Prior to this study, only two laboratory studies detailed the kinetics of Mn and N reactions and provided mechanistic insight (Cavazos et al. 2018; Luther and Popp 2002). However, the products of some Mn and N reactions have been more widely examined. For reactions with reduced nitrogen compounds, Luther et al. (1997) reacted a Mn^{III} bistris complex with ammonia, NH_3 , and found reduction of Mn(III) to Mn(II). In that work, the reaction of a Mn^{III} bistris complex with hydrazine, N_2H_4 , also led to N_2 . Luther et al. (2018) documented that ammonia, NH_3 , (not NH_4^+) oxidation by soluble Mn(III) and MnO_2 are examples of HAT reactions, as proposed here for Mn(III) oxidation of HNO_2 . Similarly, the reaction of oxidized Mn with hydroxylamine (NH_2OH), an intermediate in NH_3 oxidation, to form N_2O (Liu et al. 2017; Heil et al. 2016; Zhu-Barker et al. 2015; Cavazos et al. 2018) likely occurs by HAT reactions.

As dissolved Mn(III) complexes can be abundant in a wide range of environments (e.g., Dellwig et al. 2012; Madison et al. 2013; Oldham et al. 2017b, c; Trouwborst et al. 2003; Yakushev et al. 2007), they have the potential to serve as an important control on the redox landscape of natural systems. Beyond nitrogen species, Mn(III) complexes can also oxidize ferrous iron and sulfide (Kostka et al. 1995; Oldham et al. 2015; Siebecker et al. 2015; Trouwborst et al. 2005). In fact, due to the versatility of Mn(III) as both a reductant and oxidant, its presence in the suboxic zone has been implicated in preserving suboxic zones by “titrating” downward diffusing oxygen and upward diffusing reductants (Dellwig et al. 2010; Madison et al. 2013; Trouwborst et al. 2003; Yakushev et al. 2007). We recommend coupling molecular information with more detailed kinetics and isotope experiments exploring oxidized Mn [including dissolved Mn(III)] mediated

reactions, which would permit a more refined assessment of the underlying chemical mechanisms at play and the overall importance of these reactions in sediments, soils, and oxic-anoxic transition zones.

5.0 ACKNOWLEDGMENTS

This work was supported by NSF Geobiology and Low-Temperature Geochemistry grant EAR1826940 to SDW and CMH, by NASA Earth and Space Science Fellowship NNX15AR62H and Agouron Institute Geobiology Postdoctoral Fellowship to KMS and by NSF Chemical Oceanography grant OCE-1558738 to GWL. All original rate and isotope data can be found at <https://doi.org/10.1016/j.gca.2020.11.004>. We thank the anonymous reviewers for their constructive comments.

Ethical Declaration: The authors declare that they have no known competing financial interests or personal relationships that could have appeared to influence the work reported in this paper.

6.0. REFERENCES

- Anschutz P, Sundby B, Lefrancois L, Luther GW III, Mucci A (2000) Interactions between metal oxides and species of nitrogen and iodine in bioturbated marine sediments. *Geochim Cosmochim Acta* 64:2751-2763. [https://doi.org/10.1016/S0016-7037\(00\)00400-2](https://doi.org/10.1016/S0016-7037(00)00400-2)
- Bach RD, Ayala PY, Schlegel HB (1996) A Reassessment of the Bond Dissociation Energies of Peroxides. An ab Initio Study. *J Amer Chem Soc* 118:12758-12765. <https://doi.org/10.1021/ja961838i>
- Buchwald C, Casciotti KL (2013) Isotopic ratios of nitrite as tracers of the sources and age of oceanic nitrite. *Nat. Geosci.* 6:309–313. <https://doi.org/10.1038/ngeo1745>
- Casciotti KL (2009) Inverse kinetic isotope fractionation during bacterial nitrite oxidation. *Geochim. Cosmochim. Acta* 73:2061–2076. <https://doi.org/10.1016/j.gca.2008.12.022>

- Casciotti KL (2016) Nitrite isotopes as tracers of marine N cycle processes. *Philosophical Transactions A* 374: 20150295. <https://doi.org/10.1098/20150295>
- Cavazos AR, Taillefert M, Tang Y, Glass, JB (2018) Kinetics of nitrous oxide production from hydroxylamine oxidation by birnessite in seawater. *Mar. Chem.* 202:49-57. <https://doi.org/10.1016/j.marchem.2018.03.002>
- Dellwig O, Schnetger B., Brumsack HJ., Grossart HP, Umlauf, L (2012) Dissolved reactive manganese at pelagic redoxclines (part II): Hydrodynamic conditions for accumulation. *J. Mar. Systems* 90(1):31-41. <https://doi.org/10.1016/j.jmarsys.2011.08.007>
- Dellwig O, Leipe T, Marz C, Glockzin M, Pollehne F, Schnetger B, Yakushev E, Bottcher ME, Brumsack HJ (2010) A new particulate Mn–Fe–P-shuttle at the redoxcline of anoxic basins. *Geochim. Cosmochim. Acta* 74:7100-7115. <https://doi.org/10.1016/j.gca.2010.09.017>
- Jones MR, Luther GW, Mucci A, Tebo BM (2019) Concentrations of reactive Mn(III)-L and MnO₂ in estuarine and marine waters determined using spectrophotometry and the leuco base, leucoberbelin blue. *Talanta* 200:91-99. <https://doi.org/10.1016/j.talanta.2019.03.026>
- Herszage J, dos Santos Afonso M (2003) Mechanism of hydrogen sulfide oxidation by manganese(IV) oxide in aqueous solutions. *Langmuir* 19:9684–9692.
- Hoener M, Bodi A, Hemberger P, Endres T, Kasper T (2021) Threshold photoionization shows no sign of nitril hydride in methane oxidation with nitric oxide. *Phys. Chem. Chem. Phys.* 23:1265-1272. <http://doi.org/10.1039/d0cp04924g>
- Karolewski JS, Sutherland K., Hansel CM, Wankel SW (2021) An isotopic study of abiotic nitrite oxidation by ligand-bound manganese (III). *Geochim. Cosmochim. Acta* 293:365–378. <https://doi.org/10.1016/j.gca.2020.11.004>
- Kostka J, Luther GW III, Nealson KH (1995) Chemical and Biological reduction of Mn(III)-pyrophosphate complexes: Potential importance of dissolved Mn(III) as an environmental oxidant. *Geochim. Cosmochim. Acta* 59:885-894. [https://doi.org/10.1016/0016-7037\(95\)00007-0](https://doi.org/10.1016/0016-7037(95)00007-0)
- Klewicki JK, Morgan JJ (1998) Kinetic Behavior of Mn(III) Complexes of Pyrophosphate, EDTA, and Citrate. *Environ. Sci. Technol.* 32:2916-2922. <https://doi.org/10.1021/es980308e>
- Lin H, Taillefert M (2014) Key geochemical factors regulating Mn(IV)-catalyzed anaerobic nitrification in coastal sediments. *Geochim. Cosmochim. Acta* 133:17-33. <https://doi.org/10.1016/j.gca.2014.01.025>
- Liu S, Berns A, Vereecken H, Wu D, Brüggemann (2017) Interactive effects of MnO₂, organic matter and pH on abiotic formation of N₂O from hydroxylamine in artificial soil mixtures. *Sci. Rep.* 7:39590. <https://doi.org/10.1038/srep39590>

Luther GW III (2004) Kinetics of the reactions of water, hydroxide ion and sulfide species with CO₂, OCS and CS₂: frontier molecular orbital considerations. *Aquat. Geochem.* 10:81-97. <https://doi.org/10.1023/B:AQUA.0000038957.18584.b0>

Luther GW III, Popp JI (2002) Kinetics of the abiotic reduction of polymeric manganese dioxide by nitrite: an anaerobic nitrification reaction. *Aquat. Geochem.* 8:15-36. <https://doi.org/10.1023/A:1020325604920>

Luther GW III (2016) *Inorganic Chemistry for Geochemistry and Environmental Sciences: Fundamentals and Applications*. John Wiley & Sons Ltd., London, 456 pages. <https://onlinelibrary.wiley.com/book/10.1002/9781118851432>

Luther GW III, Sundby B, Lewis BL, Brendel PJ, Silverberg N (1997) Interactions of manganese with the nitrogen cycle: alternative pathways to dinitrogen. *Geochim. Cosmochim. Acta* 61:4043-4052. [https://doi.org/10.1016/S0016-7037\(97\)00239-1](https://doi.org/10.1016/S0016-7037(97)00239-1)

Luther GW III, Thibault de Chanvalon A, Oldham VE, Estes E, Tebo BM, Madison AS (2018) Reduction of manganese oxides: thermodynamic, kinetic and mechanistic considerations for one- versus two-electron transfer steps. *Aquat. Geochem.* 24:257-277. <https://doi.org/10.1007/s10498-018-9342-1>

Madison AS, Tebo BM, Mucci A, Sundby B, Luther GW III (2013) Abundant Mn(III) in porewaters is a major component of the sedimentary redox system. *Science* 341:875-878. <https://dx.doi.org/10.1126/science.1241396>

Matocha CJ, Sparks DL, Amonette JE, Kukkadapu RK (2001) Kinetics and mechanism of birnessite reduction by catechol. *Soil Sci Soc Am J* 65:58–66. <https://doi.org/10.2136/sssaj2001.65158x>

Oldham VE, Owings SM, Jones M, Tebo BM, Luther GW III (2015) Evidence for the presence of strong Mn(III)-binding ligands in the water column of the Chesapeake Bay. *Mar. Chem.* 171:58-66. <https://dx.doi.org/10.1016/j.marchem.2015.02.008>

Oldham VE, Jones M, Tebo BM, Luther GW III (2017a) Oxidative and reductive processes contributing to manganese cycling at oxic-anoxic interfaces. *Mar. Chem.* 195:122-128. <https://dx.doi.org/10.1016/j.marchem.2017.06.002>

Oldham VE, Mucci A, Tebo BM, Luther GW III (2017b) Soluble Mn(III)-L complexes are ubiquitous in oxygenated waters and stabilized by humic ligands. *Geochim. Cosmochim. Acta* 199:238-246. <https://dx.doi.org/10.1016/j.gca.2016.11.043>

Oldham VE, Miller MT, Jensen LT, Luther GW III (2017c) Revisiting Mn and Fe removal in humic rich estuaries. *Geochim. Cosmochim. Acta* 209:267-283. <https://dx.doi.org/10.1016/j.gca.2017.04.001>

- Owings SM, Luther GW III, Taillefert M (2019) Development of a rate law for arsenite oxidation by manganese oxides. *Geochim. Cosmochim. Acta* 250:251-267. <https://doi.org/10.1016/j.gca.2019.02.003>
- Qian A, Zhang W, Shi C, Pan C, Giammar DE, Yuan S, Zhang H, Wang Z (2019) Geochemical Stability of Dissolved Mn(III) in the Presence of Pyrophosphate as a Model Ligand: Complexation and Disproportionation. *Environ. Sci. Technol.* 53:5768-5777. <https://doi.org/10.1021/acs.est.9b00498>
- Siebecker MG, AS Madison, Luther GW III (2015) Reduction Kinetics of Polymeric (Soluble) Manganese (IV) Oxide (MnO₂) by Ferrous Iron (Fe²⁺). *Aquatic Geochemistry* 21(2-4):143-158. <http://dx.doi.org/10.1007/s10498-015-9257-z>
- Stone AT, Morgan JJ (1984a) Reduction and dissolution of manganese (III) and manganese(IV) oxides by organics. 1. Reaction with hydroquinone. *Environ Sci Technol* 18:450-456.
- Stone AT, Morgan JJ (1984b) Reduction and dissolution of manganese (III) and manganese(IV) oxides by organics. 2. Survey of the reactivity of organics. *Environ Sci Technol* 18:617-624.
- Trouwborst RE, Clement BG, Tebo BM, Glazer B, Luther GW III (2006) Soluble Mn(III) in suboxic zones. *Science* 313:1955-1957. <https://doi.org/10.1126/science.1132876>
- Watters JL, Kolthoff IM (1948) Potentiometric Investigation of Tripyrophosphatomanganic (III) Acid. *J. Amer. Chem. Soc.* 70:2455-2460.
- Yakushev E, Pollehne F, Jost F, Kuznetsov I, Schneider B, Umlauf L (2007) Analysis of the water column oxic/anoxic interface in the Black and Baltic seas with a numerical model. *Mar. Chem.* 107:388-410. <https://doi.org/10.1016/j.marchem.2007.06.003>
- Yao W, Millero FJ (1993) The rate of sulfide oxidation by δ MnO₂ in seawater. *Geochim. Cosmochim. Acta* 57:3359-3365. [https://doi.org/10.1016/0016-7037\(93\)90544-7](https://doi.org/10.1016/0016-7037(93)90544-7)
- Yao W, Millero FJ (1995) Oxidation of hydrogen sulfide by Mn(IV) and Fe(III) (hydr)oxides in seawater. In: Vairavamurthy V, Schoonen MAA, Eglinton TI, Luther GW, Manowitz B (eds) *Geochemical transformations of sedimentary sulfur*. American chemical society symposium series, vol 612, Ch. 14. Washington, DC, pp 260-279.
- Zhang X-M, Bordwell FG (1992) Homolytic bond dissociation energies of the benzylic C-H bonds in radical anions and radical cations derived from fluorenes, triphenylmethanes, and related compounds. *J Am Chem Soc* 114:9787-9792.
- Zhu-Barker X, Cavazos AR, Ostrom NE, Horwarth WR, Glass JB (2015) The importance of abiotic reactions for nitrous oxide production. *Biogeochemistry* 126:251-267. <https://doi.org/10.1007/s10533-015-0166-4>